Sensorized laparoscopic surgical grasper with integrated capacitive force sensor for robot-assisted minimally invasive surgery

Muhammad Ameer Usman, Rehan Muhammad, Taimoor Shabbir, Mohsin Islam Tiwana, Amir Hamza and Muhammad Mubasher Saleem

Department of Mechatronics Engineering, National University of Sciences and Technology, Islamabad, Pakistan

Abstract

Purpose – This paper aims to introduce a sensorized surgical grasper with a novel flexible capacitive tactile force sensor integrated within the surgical grasper for minimally invasive surgery (MIS) and robot-assisted MIS (RMIS) procedures.

Design/methodology/approach – The proposed sensor offers a unique configuration of sensing electrodes with one top excitation electrode and three bottom electrodes enabling the measurement of normal and shear forces without incorporating any complex decoupling algorithms. The design of the sensor is optimized using finite-element method simulations, ensuring efficiency and reliability.

Findings – Experimental validation, real-time sensor response and application in lump detection through stiffness assessment demonstrate the decoupled force response (0–5 N normal range and 0–2 N shear range) with high sensitivity 0.0124/N, repeatability and hysteresis response with 5.65% and 4.7% errors respectively.

Originality/value – The compact design of the sensor makes it compliant with surgical graspers and therefore enhances the overall efficiency of robotic surgical procedures. The sensorized surgical grasper is fabricated using conventional machining and rapid prototyping techniques, presenting a cost-effective solution for adoption.

Keywords Rapid prototyping, Robotic surgery, Flexible capacitive tactile sensor, Sensorized grasper, Stiffness assessment

Paper type Technical paper

1. Introduction

Tactile feedback and force sensing are of vital importance so that humans can effectively understand human – machine interactions. The measurement of the characteristics such as temperature, softness, texture, shape, size, composition and shear and normal forces refers to as tactile feedback whereas force sensing only refers to the measurement of magnitudes of shear and normal forces (Tiwana *et al.*, 2012).

Robotic minimally invasive surgery (RMIS) has revolutionized the medical technology (Rivero-Moreno *et al.*, 2023), owing to its countless patient benefits, including reduced postoperative pain, recovery duration and the overall cost of medical care. The major benefits of RMIS are less scarring, diminished risk of infection, less blood loss and minimum recovery time (Bechet *et al.*, 2015; Lanfranco *et al.*, 2004). The main challenge faced by the surgeons in RMIS is the absence of tactile sensation which can limit the efficiency of surgical procedures. Many reports confirm that due to the lack of tactile sensation excessive forces in robotic surgery cause tissue damage and post-surgery complications (Barrie *et al.*, 2018; Simaan *et al.*, 2018). Tactile sensation is crucial for surgeons to safely handle tissues, organs and sutures and assess the thickness as well as texture of tissues (Alleblas *et al.*, 2017; Sastry *et al.*, 1997). Many researchers have made various attempts to achieve force feedback to address above issues by developing and integrating tactile sensors within palpation probes (Kim *et al.*, 2018a; Naidu *et al.*, 2017), and sensorized surgical forceps (Kim *et al.*, 2015; Lee *et al.*, 2016; Yu *et al.*, 2018).

Generally, force sensor-integrated surgical instruments are mainly classified based on the locations on which the sensor is mounted (Lee *et al.*, 2016). In this study, the focus is mainly on the grasper-integrated tactile sensors. Previously, tactile sensors have mainly relied on sensing modalities like piezoresistive (Karmakar *et al.*, 2022; Takahashi *et al.*, 2013), piezoelectric (Dargahi, 2000), magnetic (Chatzipirpiridis *et al.*, 2015; Rehan *et al.*, 2022), capacitive (Hussain *et al.*, 2024; Kim *et al.*, 2011; Zhu *et al.*, 2022) and optical sensing (Li *et al.*, 2018; Wanninayake, 2019). Although optical sensors offer remarkable accuracy and sensitivity, their adoption in medical applications is hindered by their high cost, distal mounting and size (Roriz *et al.*, 2013). On the other hand, piezoresistive tactile sensors are cost-effective and easy to build but suffer from significant mechanical hysteresis (Bandari *et al.*, 2020). Piezoelectric tactile sensors offer impressive sensitivity and accuracy but come with certain limitations, they are good to measure dynamic forces while in

The current issue and full text archive of this journal is available on Emerald Insight at: **https://www.emerald.com/insight/0260-2288.htm**

Sensor Review
 [ISSN 0260-2288]
[DOI 10.1108/SR-09-2024-0765]

This work was supported and funded by the Higher Education Commission (HEC), Pakistan and British Council UK within the framework of the Innovative and Collaborative Research Partnerships Grants (ICRG) program under the project. No. ICRG-147.

Received 9 September 2024
Revised 27 November 2024
Accepted 14 December 2024

tactile sensing static forces need to be measured, they are sensitive to temperature and have limited tactile spatial resolution and hysteresis (Krishna and Rajanna, 2025; Najarian *et al.*, 2006).

Among these options, capacitive tactile sensors stand out as the preferred choice for electrical-based sensors in RMIS. They are flavored due to their simple device structure, low power consumption, excellent detection capabilities even at low force levels, rapid response to dynamic changes, low-cost and overall durability. These sensors can be integrated into various surgical tools, including probes for palpation tasks and graspers for force feedback (Hsieh *et al.*, 2021; Othman *et al.*, 2022a).

(Sedaghati *et al.*, 2005) proposed a piezoelectric tactile force sensor for endoscopic grasper. The sensor was capable of measuring contact forces with high sensitivity and good linearity. In another study, (Sokhanvar *et al.*, 2007) proposed a PVDF (Polyvinylidene Fluoride) based tactile force sensor for surface roughness and compliance measurement for specific surgical tools like endoscopic graspers and robotic end effectors. (Tanaka *et al.*, 2000) proposed a palpation sensor probe for prostatic cancer detection and palpation. The proposed sensor was mounted on the tip of the palpation probe and the transduction mechanism of the sensor was piezoelectric based. Force magnitude and force orientation are fundamentally important for an adequate tactile sensor design (Dargahi, 2000). (Dai *et al.*, 2017) introduced a tri-axis force sensor characterized by excellent force measurement capabilities. To achieve this, they consciously disregarded size limitations, leading to an expansion of the sensing unit area. Therefore, the data acquisition circuitry extended beyond the grasper boundaries, exposing the capacitance chip and wires to the external environment. Unfortunately, this design choice renders the instrument unsuitable for use during surgical procedures, as the surrounding environment significantly influences the capacitance and compromises the sensor's accuracy. (King *et al.*, 2009) devised a piezoresistive tactile sensor that was incorporated on the tip of a surgical instrument, although piezoresistive sensors have high immunity toward noise and are also highly sensitive, manufacturing methods for multi-axis piezoresistive devices can be complex. In another development, (Lee *et al.*, 2025) introduced a multi-axis contact force sensor with normal and shear force measurement capabilities. However, achieving accurate contact force information with this sensor was challenging due to issues related to nonlinearity, size, poor resolution and intricate calibration procedures. (Kim *et al.*, 2018b) integrated the sensor at the proximal region to minimize the grasper size, but the proximal region may contact the other parts of the body during surgery, resulting in distorted force feedback. (Othman *et al.*, 2022b) integrated a force sensitive resistor (FSR) at the tip of the surgical grasping tool to measure the forces and for lump detection within tissues, however, FSR is very susceptive to noise and the issue of exposed sensing elements along with wires makes the tool unsuitable for surgical use.

Although sensorized graspers with integrated tactile force sensors have been developed, these tactile force sensors have their inherited issues of design complexity, manufacturing complications, intricate calibration processes or usability during surgical procedures. The literature on sensorized graspers shows that the development of tactile force sensors with the capability of integrating with laparoscopic graspers is a difficult task due to constraints such as the size, range, resolution and location of the sensor. Decoupling force into its normal and shear components is crucial for force feedback in RMIS, as it enables precise tissue characterization and enhances grasping stability.

In this study, a low-cost flexible capacitive tactile force sensor is introduced, featuring a distinctive electrode configuration and eliminating the need to decouple the forces, as the sensor's design makes it capable of measuring both normal and shear force effectively with minimal interference of both forces on each other. The focus is on small size, high force range, high sensitivity, minimal hysteresis error and good repeatability. The sensorized grasper is designed by integrating the flexible capacitive tactile force sensor in the designed laparoscopic surgical tool. Due to its small size, simple structure and easy configuration, the proposed sensor can easily be assembled into robotic and conventional surgical graspers while preserving the integrity of the force feedback with minimal complications.

2. Sensor design and working principle

Figure 1 shows the schematic of the proposed grasper-integrated flexible capacitive tactile force sensor. It comprises of three lower electrodes named C_{y-}, C_z and C_{y+}. The upper electrode is an excitation electrode. The capacitance change occurs between the C_z electrode and excitation electrode due to the decreasing thickness of the dielectric elastomer upon applied normal force F_n, the cross-sectional view of the sensor under F_n is shown in Figure 2(b). The differential change in capacitance occurs between C_j electrodes, where j is $y-$ and $y+$, due to the change in overlapping area of the C_j and excitation electrodes upon applied shear force F_s, the cross-sectional view of the sensor under F_s is shown in Figure 2(c). The sensor is fabricated using a Flexible Printed Circuit Board (FPCB), the dimensions of the excitation, C_z and C_j electrodes are shown in Table 1. The spacings between the lower electrodes are 0.5 mm.

Figure 1 Schematic diagram of the proposed flexible capacitive tactile force sensor (top view)

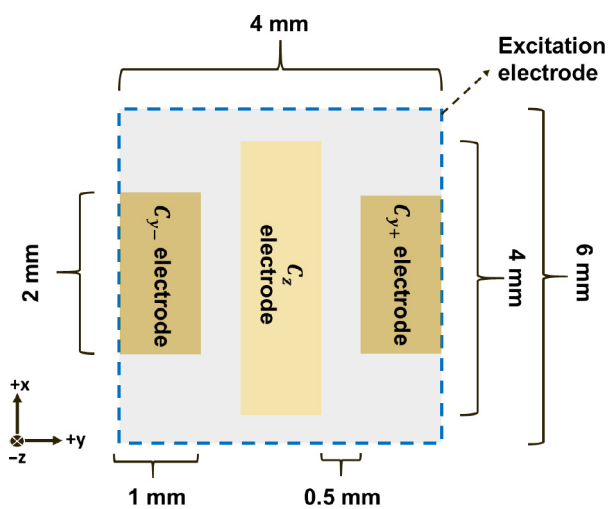

Source: Figure by authors

Figure 2 Structure and sensing principles of the proposed sensor (a) cross-sectional view (b) behaviour under normal force. (c) Behavior under shear force. (d) Behavior under normal and shear forces (e) 3D model of the proposed surgical grasper with the integrated flexible capacitive tactile force sensor

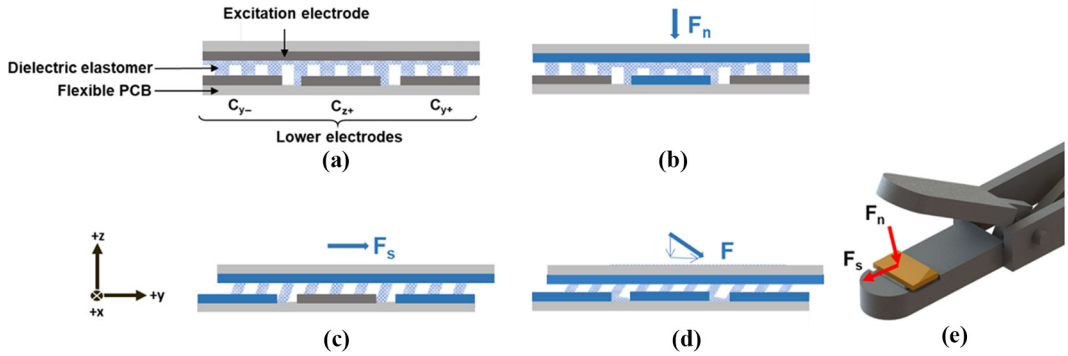

Source: Figure by authors

This unique electrode configuration uses two distinct sensing schemes, one for normal force and one for shear force, ensuring minimal mutual interference. In this study, we have effectively mitigated the impact of horizontal forces in x-direction on normal force measurements by designing the lower electrodes (C_z, C_j) to be smaller than the excitation electrode, as illustrated in Figure 1. This design choice eliminates any potential influence of capacitance changes due to alterations in the overlapping area when dealing with normal forces.

The proposed flexible capacitive tactile force sensor implements two different sensing schemes one for normal force and the second for the shear force. The capacitance change can occur either through changes in the overlap area between the electrodes or changes in the thickness of the dielectric elastomer situated between the electrodes. For the measurement of normal force F_n, we used the working mechanism that is based on the change of thickness of dielectric elastomer between electrodes. Therefore, the general relation between capacitance and thickness can be written as $C = \frac{\varepsilon_r \varepsilon_o A}{d}$, where C represents capacitance, A is the overlapping area between the upper and lower electrodes, d is the thickness, ε_o represents the dielectric constant of air and ε_r represents relative permittivity of dielectric elastomer. Figure 2(a) shows that the change in thickness of elastomer changes the gap between the excitation electrode and C_z electrode, which causes a capacitance change between electrodes. The capacitance can be written as an equation of normalized capacitance change by subtracting the nominal capacitance from the capacitance after force application. The change in capacitance due to the initial (nominal) gap d_1 and the final gap d_2 can be written as:

Table 1 Dimensions of electrodes for the proposed flexible capacitive tactile force sensor

	EXC	C_z	C_j
Length (mm)	6	4	2
Width (mm)	4	1	1

Source: Table by authors

$$\Delta C_n = \varepsilon_r \varepsilon_o A \left(\frac{1}{d_2} - \frac{1}{d_1} \right) \quad (1)$$

Equation (1) is used for the measurement of normalized capacitance change for normal force, where A is constant because the overlap area will never change between the excitation electrode and C_z electrode even during shear force.

The differential capacitance is used to measure shear force F_s, the overlap area of the excitation electrode and C_j electrodes changes which will cause a change in capacitance as shown in Figure 2(c). The equation for the measurement of the differential capacitance change can be expressed as $\Delta C_s = \varepsilon_r \varepsilon_o \left(\frac{A_{y+}}{d_{y+}} - \frac{A_{y-}}{d_{y-}} \right)$, where, ΔC_s stands for differential capacitance due to shear force between C_j electrodes, A_j represents the overlap area of the C_j electrodes and excitation electrode, d_j represents the thickness of dielectric elastomer between the C_j electrodes and excitation electrode, where j is $y-$ and $y+$.

In Figure 2(c), for the force in $+y$-axis, the overlapping area between the excitation electrode and C_{y-} electrode changes while the overlap area between excitation and C_{y+} remains constant, also for the force in -y-axis, the overlap area between the excitation electrode and C_{y+} electrode changes while the overlap area between excitation and C_{y-} remains constant. Therefore, the modified equation for differential capacitance under shear force F_s can be written as:

$$\Delta C_s = \varepsilon_r \varepsilon_o \left(\frac{A_{y+} - \delta A_{y+}}{d_{y+}} - \frac{A_{y-} - \delta A_{y-}}{d_{y-}} \right) \quad (2)$$

In equation (2), δA_{y+} represents the change in the overlap area between C_{y+} and excitation electrodes and δA_{y-} represents the change in the overlap area between C_{y-} and excitation electrodes.

3. Fabrication of grasper-integrated force sensor

The proposed grasper-integrated flexible capacitive tactile force sensor comprises the following parts: an upper plate with an excitation electrode, a FPCB with embedded electronics and lower electrodes (C_{y-}, C_z, C_{y+}), and a lower grasper base structure. FPCB has three lower electrodes and AD7746

capacitance to digital converter (CDC) chip. The sensing area of the proposed sensor is 24 mm^2. Figure 3 illustrates the various stages involved in the fabrication process of the sensorized grasper. The FPCB for the proposed sensor is manufactured by a PCB manufacturing company. The electronics components (decoupling capacitors and CDC) and the connecting wires (for power and communication) are soldered onto the FPCB via surface mount technology.

The dielectric elastomer material used for the proposed sensor is Smooth-On Ecoflex 00–30 silicone rubber. The liquid silicone rubber is procurable in two parts which are blended in equal volumetric ratios for 3 min, after degassing, the mixture is poured into the 3 D printed Polylactic Acid molds and left for curing under room temperature for 4 h. After the elastomer is cured, it is glued to the FPCB sensing area (on the lower electrodes). The excitation electrode embedded on the upper plate is glued to the top of the dielectric elastomer. In the next step, the CDC chip cover is glued above the electronics which also serves as the grasping surface. The exploded view of the sensorized laparoscopic grasper is shown in Figure 4(a) and finally, the assembled grasper is shown in Figure 4(b).

4 Finite-element method modelling

An electromechanics finite-element method (FEM) analysis is carried out to determine the optimal shape of the dielectric elastomer and to examine its deformation under applied normal and shear forces. This multiphysics analysis couples electrostatic and solid mechanics modules for a coupled analysis to simulate capacitance changes based on the displacement due to applied force. The solid mechanics module incorporates the nodal displacements by using first Piola-Kirchoff equation $(0) = \nabla(FS)^T + \boldsymbol{F}_v$ where $F = \mathrm{I} + \nabla\mathbf{u}$ is deformation gradient, S is the stress gradient, $\boldsymbol{F}_v$ is the applied volumetric force, I represents the identity matrix and $\mathbf{u}$ is the displacement field of the sensor. The electrostatics model incorporates Maxwell's capacitance matrix $[Q_{ij}] = [C_{ij}][V_{ij}]$ to calculate the capacitances of the sensor based on the charge accumulated between the electrodes. The material properties of the dielectric elastomer presented in (Vaicekauskaite *et al.*, 2020)

Figure 4 (a) Exploded view of sensorized forceps (b) fabricated and assembled sensorized grasper

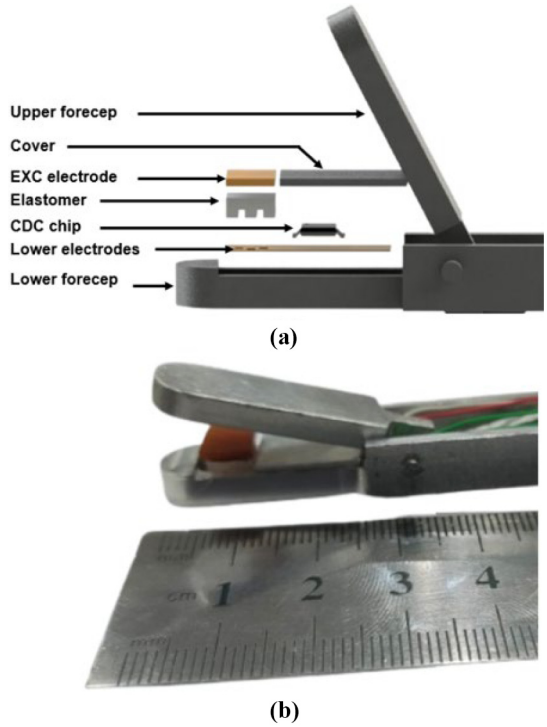

Source: Figure by authors

are used for the analysis. The square symmetric rigid plate with FR4 material is used to apply uniform forces (normal and shear) on the sensor.

Solid mechanics analysis is carried out with patterned as well as a solid dielectric elastomer. Figure 5(a) and (b), show the displacement profile under uniformly distributed normal force on the sensor with patterned and solid dielectric elastomer respectively. Figure 5(c) shows the displacement vs normal force plot. Figure 6(a) and (b) show the displacement profile

Figure 3 Fabrication stages of the proposed sensorized grasper

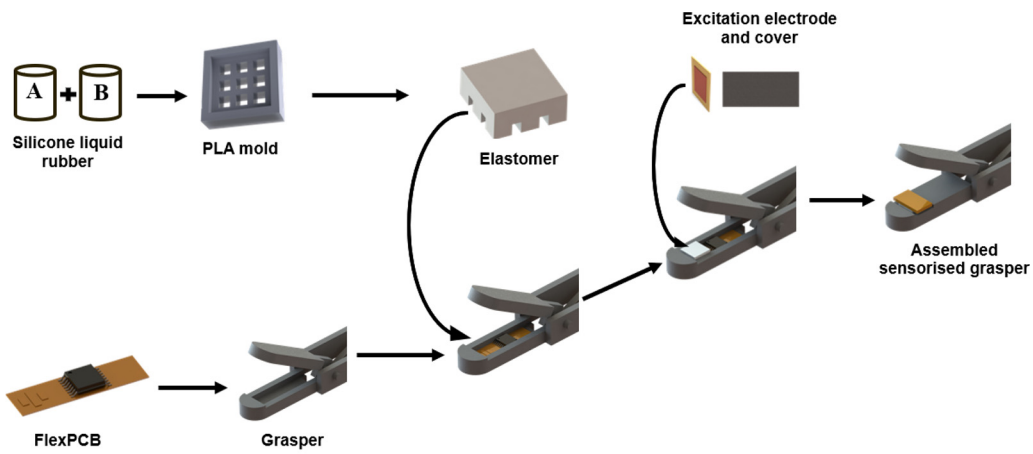

Source: Figure by authors

Figure 5 Displacement response of the sensor under normal force (a) displacement profile with solid elastomer (b) displacement profile with patterned elastomer (c) displacement comparison between patterned and solid elastomers under applied normal force plot

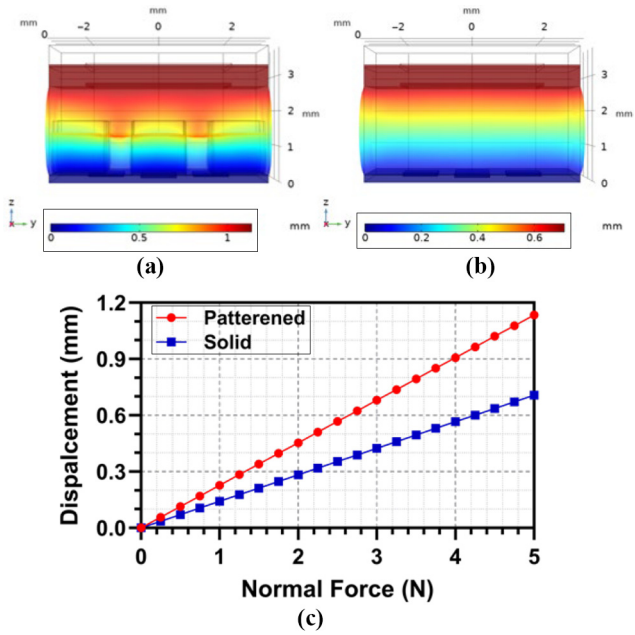

Source: Figure by authors

Figure 6 Displacement response of the sensor under shear force (a) displacement profile with solid elastomer(b) displacement profile with patterned elastomer (c) displacement comparison between patterned and solid elastomers under applied normal force plot

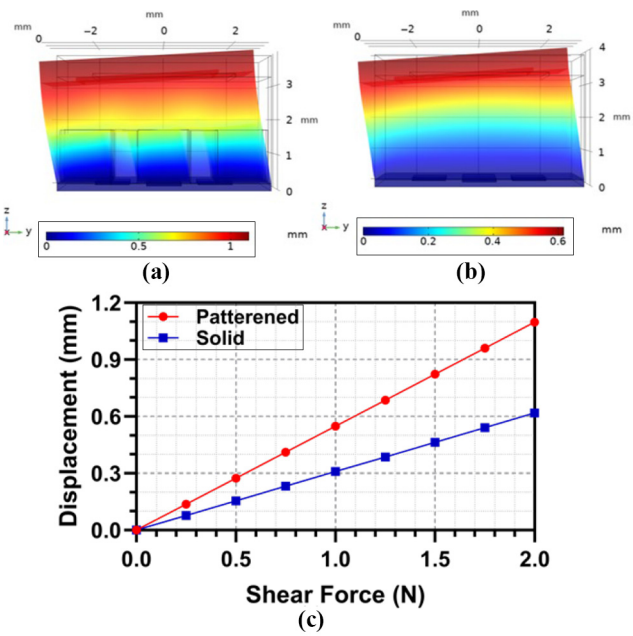

Source: Figure by authors

under applied shear force on the sensor with patterned and solid dielectric elastomer respectively. Figure 6(c) shows the displacement vs shear force plot. It can be seen from the plots that for solid elastomer the displacement is smaller for applied force as compared to the displacement of patterned elastomer. Based on the displacement plots under normal and shear forces shown in Figure 5(c) and Figure 6(c), the displacement reaches approximately 1 mm when subjected to a normal force of 5 N and a shear force of 2 N. These values represent the maximum permissible displacement limits as per the design specifications.

The working principle of the sensor under applied normal and shear force is validated with electromechanics module. Figure 7(a) and (b) show the normal and differential capacitance change due to normal and shear displacement respectively. The normalized capacitance change ΔC_z increases uniformly with the normal displacement of elastomers, whereas it also shows that the normalized differential capacitance change remains almost zero i.e. $\Delta C_y = 0$. The differential capacitance ΔC_y increases uniformly with the shear displacement of elastomers, whereas it also shows the normal capacitance remains zero i.e. $\Delta C_z = 0$.

5. Experimental setup and data acquisition

The experimental setup includes a tri-axis translation stage for applying forces to the fabricated proposed sensor (Figure 8).

Figure 7 Force vs Capacitance response for differential capacitance ΔC_y and normal capacitance ΔC_z

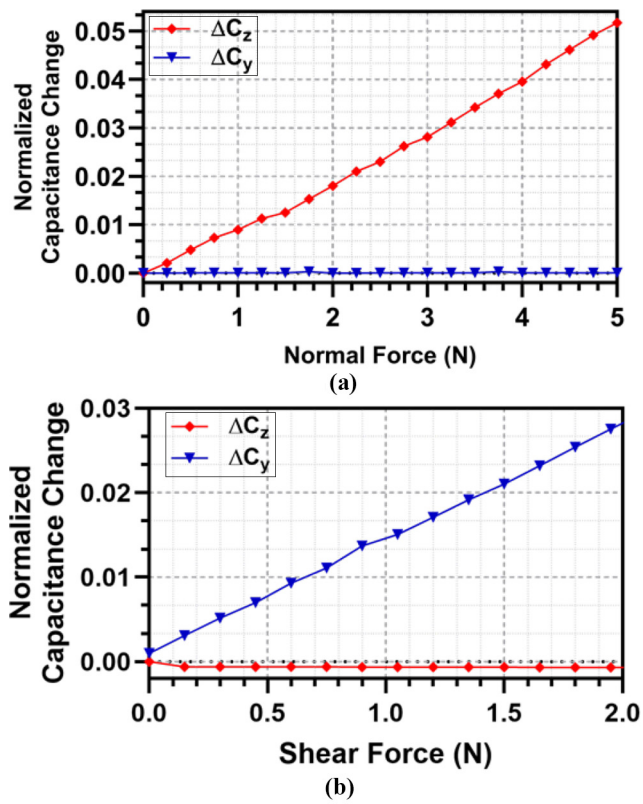

Notes: (a) Under applied normal force; (b) under applied shear force
Source: Figure by authors

Figure 8 Experimental setup for calibration and characterization of the proposed sensor

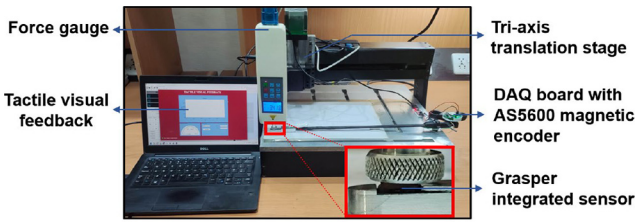

Source: Figure by authors

Additionally, the setup features a digital push-pull force gauge to measure the applied force on the sensor, with a maximum force range of 10 N and a resolution of 1 mN.

The force gauge is mounted on a 3D printed fixture made of PLA, which is fixed on the moveable end of the tri-axis translation stage. The force gauge is mounted on the translation stage in a vertical orientation to measure the applied normal force along the z-axis. For measuring force along the y-axis when shear force is applied, the force gauge is positioned horizontally on the translation stage. The tri-axis translation stage is controlled using CNC software graphical user interface of the computer.

The data acquisition schematic is shown in Figure 9. The bottom electrodes of the capacitive sensor are etched on an FPCB and a high resolution (4 aF), high precision (4 fF) CDC (AD7746) is assembled on the same FPCB for differential and single-ended capacitance data acquisition from the sensor. The excitation electrode is excited through the *EXCA* pin. The differential capacitance of electrodes C_j, where j is $y-$ and $y+$, is measured across the differential channels C_{1+} and C_{1-} and the single-ended capacitance of the electrode C_z is measured across the single-ended channel C_{2+}. The measured capacitance is balanced by programmable on-chip digital-to-capacitance converter CAPDACs using internal negative capacitors connected to the capacitive channels for offset calibration.

5.1 Normal force characterization

The normalized change in capacitance for an applied normal force is illustrated in Figure 10. As the elastomer undergoes maximum deformation, the upper plate reaches its peak displacement, causing the sensor output to saturate. The nominal capacitance for the proposed sensor is recorded as 0.1455 pF. The sensor demonstrates a maximum force range of 5 N, with a sensitivity of 0.0124/N and an R^2 value of 0.9802, indicating a highly linear response to the applied normal force. In the FEM simulation at 5 N applied normal force ΔC_z is 0.0517 and that for experimental results is 0.0619. The difference between simulated and experimental results occurs mainly due to misalignment of the electrodes, external noise and lack of hyper-elasticity consideration during simulation.

5.2 Shear force characterization

The normalized capacitance changes for an applied shear force in the $-y$ direction is shown in Figure 11. The noted nominal capacitance for the proposed sensor is 0.0274 pF. A maximum force range of 2 N with a sensitivity of 0.0205/N and R^2 value of 0.9934 which indicates highly linear response, is noted for the applied shear force. In the FEM simulation at 2 N applied shear

Figure 10 Force vs Normalized capacitance change under normal force

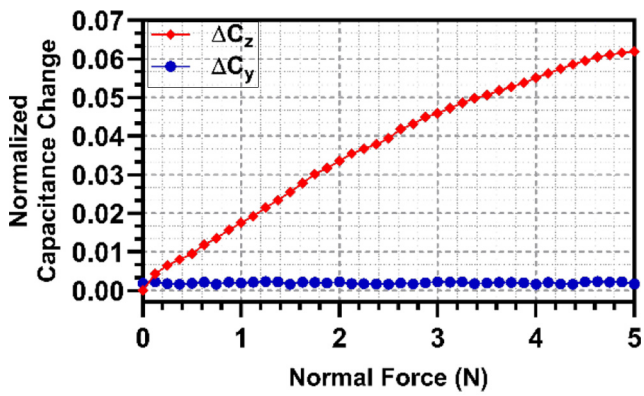

Source: Figure by authors

Figure 9 Schematic diagram of the data acquisition of proposed sensor and the magnetic encoder

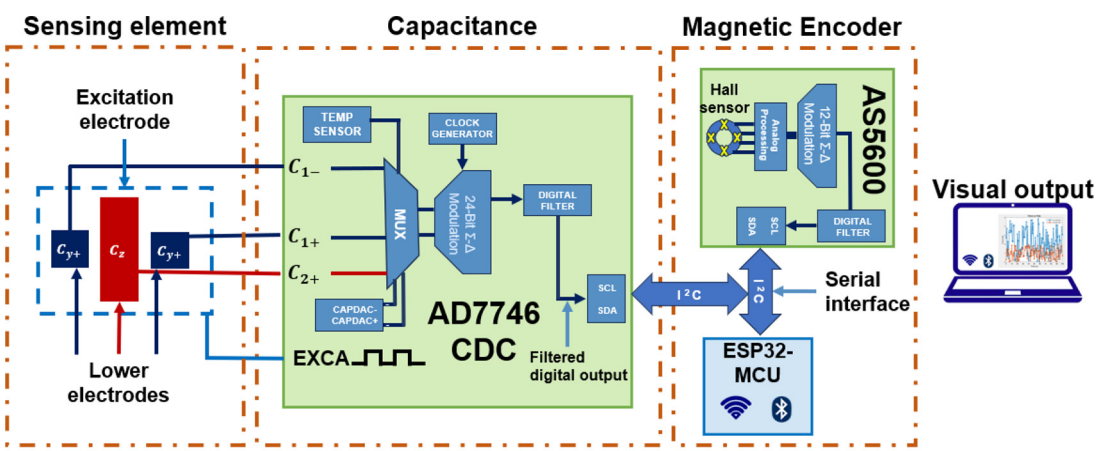

Source: Figure by authors

Figure 11 Force vs. Normalized capacitance change under shear force

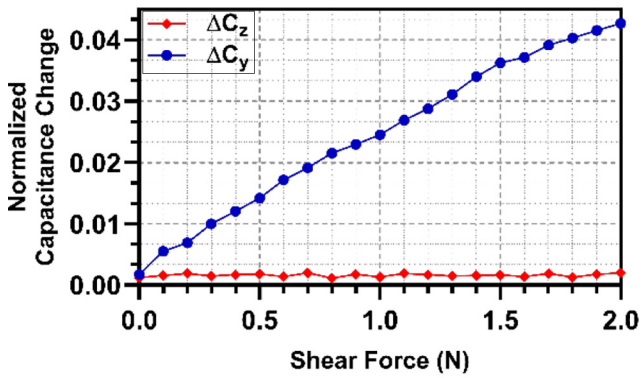

Source: Figure by authors

force ΔC_y is 0.0296 and that for experimental results is 0.0427 indicating that the simulated and experimental results have similar response to each other validating the proposed sensor design. The reasons for the difference occurring between simulation and experimental results are discussed in the previous section.

5.3 Estimating force using the measured change in capacitance

A mathematical model is required to convert the sensor's measured capacitance into force estimates, enabling the sensor to function effectively in real-world applications. The proposed sensor undergoes calibration across the full range of applied normal and shear forces, resulting in second-order polynomial expressions derived through curve fitting. The final expressions for force estimation based on the normalized change in capacitance for both normal and shear directions are as follows:

$$\Delta C_z = -0.001304F_n^2 + 0.018900F_n + 0.000617 \quad (3)$$

$$\Delta C_y = -0.002638F_s^2 + 0.025910F_s + 0.002154 \quad (4)$$

Where ΔC_z represents the change in capacitance in the normal direction resulting from the application of a normal force, and ΔC_y represents the change in capacitance in the shear direction caused by the application of a shear force. The variable F_n and F_s denotes the magnitude of the applied normal force and shea force respectively.

Figure 12(a) and (b) present a comparison between the applied force and the estimated force, calculated using the developed analytical expressions, for both normal and shear forces when applied to Ecoflex 00–30. The graphs show a strong correlation, validating the precise estimation of the applied force on the sensor through the observed changes in output capacitance. The RMS error values for the applied and estimated normal force and shear force are 4.961% and 2.337% respectively.

6. Real-time sensor feedback during tissue manipulation

The proposed sensorized grasper equipped with an integrated capacitive tactile force sensor, is evaluated by manipulating a

Figure 12 Comparison of the applied force and the estimated force based on the measured capacitance change of the sensor using ecoflex 00–30

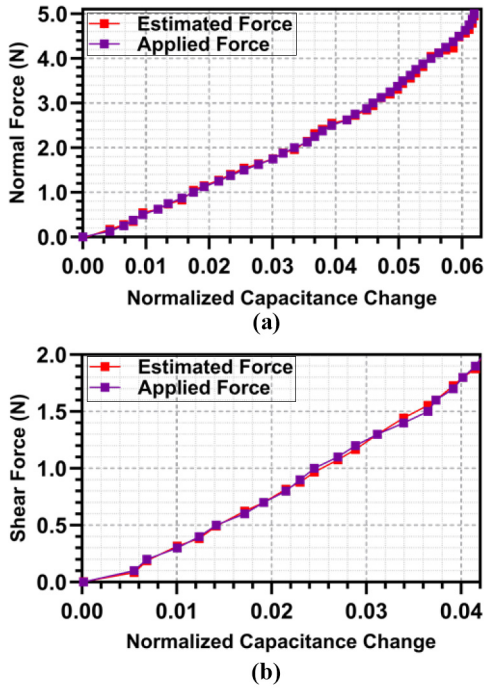

Notes: (a) Normal forc;e (b) shear y-axis force
Source: Figure by authors

simulated silicone rubber tissue. This tissue is firmly secured at one end to a steel base. The free end of the tissue is manipulated using the sensorized surgical grasper. During the tissue manipulation we recorded 200 real-time data points over the course of 30 seconds. Figure 13(a) represents the grasping force action while Figure 13(b) shows the pulling force action.

In Figure 14 the sensor response for the real-time testing is shown; Figure 14(a) represents the grasping force response and Figure 14(b) represents the pulling force response. Initially, the simulated tissue is grasped firmly and is not pulled, the grasping force increases while the pulling force

Figure 13 Real-time testing setup (a) normal force being applied by grasping (b) shear force is being applied by pulling the tissue and then slightly letting the tissue slip

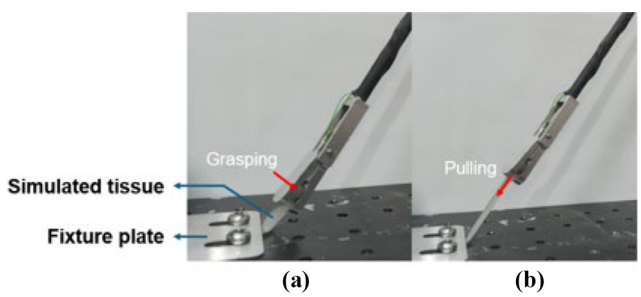

Source: Figure by authors

Figure 14 Real-time sensor response under (a) grasping force and (b) pulling force

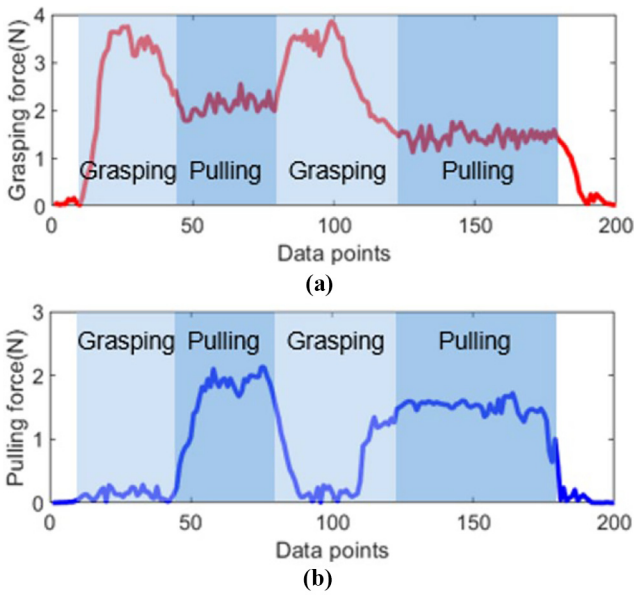

Source: Figure by authors

remains minimal, when the tissue grasp is loosened after pulling the tissue, the pulling force by the tissue on the sensor increases as the tissue pulls the sensor during slippage, which results in a decrease of grasping force and increase of pulling force. When the tissue is grasped firmly the grasping force increases while the slippage (pulling force) becomes minimal. The lighter-toned sections in Figure 14 represent the grasping action and the darker-toned sections represent the pulling action.

6.1 Stiffness assessment and lump detection

The proposed capacitive tactile force sensor is used in the application of lump detection through stiffness assessment with the method reported in the work of (Othman *et al.*, 2022b). According to (Othman *et al.*, 2022b) the angular displacement is zero when the grasper is fully open, and it is maximum when it is fully closed. Lumps are harder than the normal tissue and when a lump comes in the grasper, the grasping force becomes high for the same angular displacement when the tissue is grasped from a location where lump is not present. Similarly, the angular displacement is smaller for the tissue with lump than the angular displacement for the tissue with lump when same force is applied.

The angular displacement is measured using the AS5600 factory calibrated magnetic encoder, and the force feedback is obtained from the proposed sensor. A simulated tissue of Ecoflex 00–30 with an embedded lump of PLA is used for the stiffness assessment. Figure 15(a) represents the tissue with embedded lump along with the grasping positions. Figure 15(b) and (c) represent the grasping of the tissue from the position where lump is present and where it is not present respectively.

In this experiment single point force and angular displacement are acquired for each location and plotted. Figure 16 represents

Figure 15 (a) Simulated tissue of ecoflex 00–30 with embedded PLA lump (b) grasping from the side with lump (c) grasping from the side without lump

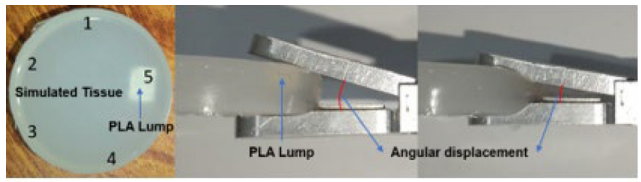

Source: Figure by authors

Figure 16 Force and angular displacement of the surgical grasper during lump detection

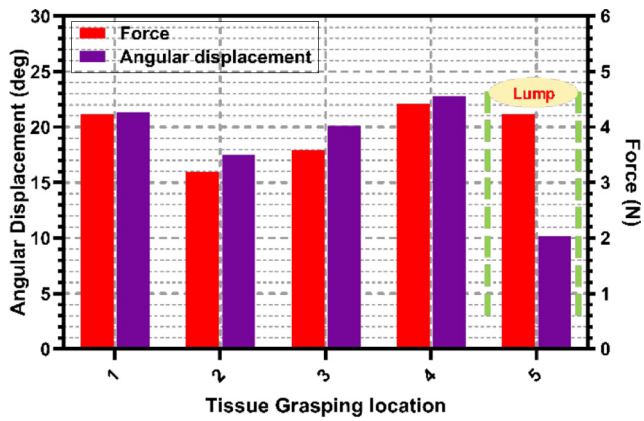

Source: Figure by authors

the angular displacement and measured force during the grasping of the simulated tissue from five different locations. Notice that when the tissue is grasped from the locations where the lump is not present, the angular displacement is greater than the angular displacement at the location where the lump is present when approximately similar force is applied.

This experiment shows the utility of the proposed capacitive tactile force sensor in lump detection via stiffness assessment when integrated with commercially available magnetic encoder.

6.2 Hysteresis and repeatability

Hysteresis error is a crucial factor in sensor characterization, as low hysteresis error ensures the sensor's suitability for applications requiring precise force feedback. Figure 17 shows the force–capacitance curves during loading and unloading for the proposed tactile force sensor, with a hysteresis error of 4.7%.

Repeatability is another key parameter for tactile sensors, particularly in robotic surgical systems. The repeatability analysis of the proposed sensor involved performing five loading cycles each day over five consecutive days. The sensor's capacitive response was measured under a 5 N normal force.

Figure 18 illustrates the test results, highlighting the average of five measurements and a minimal standard deviation represented by the error bars, all corresponding to the applied

Figure 17 Hysteresis response of the proposed tactile force sensor with ecoflex 00–30 as elastomer under normal force

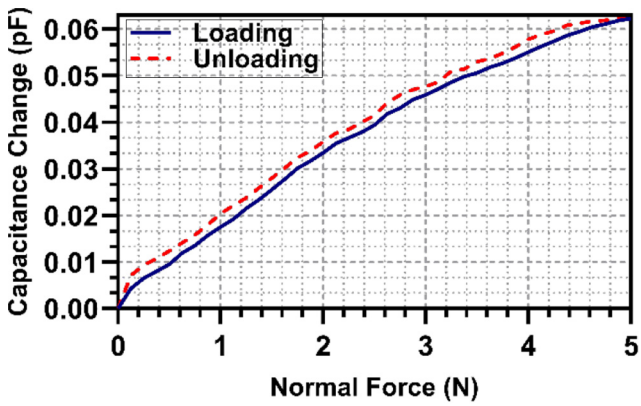

Source: Figure by authors

Figure 18 Capacitive response of the proposed tactile force sensor with ecoflex 00–30 elastomer for five loading cycles over a span of five days (error bars represent standard deviation)

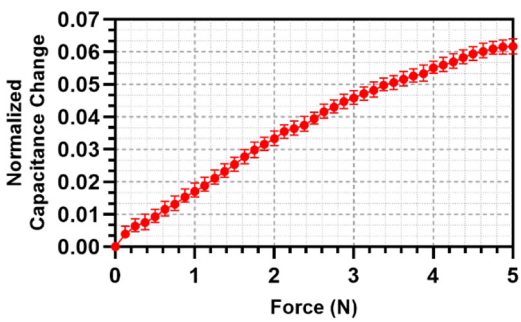

Source: Figure by authors

force. The sensor exhibited stable output with a repeatability error of 5.65%.

7. Sensor response under varying temperature

The performance of capacitive sensors is significantly influenced by temperature changes which affects both sensitivity and accuracy in force measurements. Keeping in mind the core human body mean temperature ranges between 36.69 °C ± 0.34 °C (Geneva *et al.*, 2019), the temperature fluctuation range during surgeries in the case of hypothermia is 0.5 °C–1.5 °C (Feldheiser *et al.*, 2016). To analyze the sensor response under environmental temperature variations, the sensor is placed inside an acrylic chamber and using a digital thermometer the temperature of the chamber is monitored. The temperature inside the chamber is increased using heat gun. The experimental setup for temperature response of the proposed sensor is shown in Figure 19(a). The testing temperature range for the proposed sensor is 25 °C–40 °C and the capacitance of the sensor was recorded every 1 °C increase in temperature. The sensor was

Figure 19 Change in base capacitances (normal and shear) with 0 N applied force under a temperature range of 25 °C–40 °C

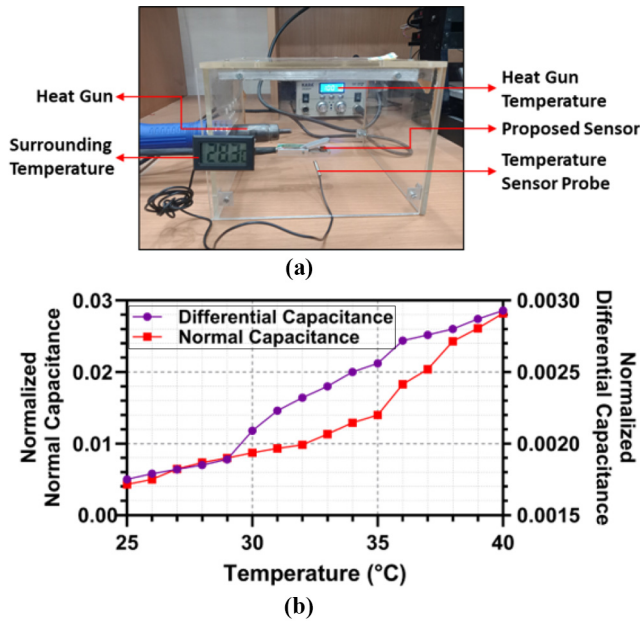

Source: Figure by authors

placed in the acrylic chamber to record the normalized base capacitance (for C_z and C_j electrodes) changes.

Figure 19(b) represents the normalized capacitance change due to increasing temperature. The base capacitance value for C_z and C_j electrodes at 25 °C is recorded to be 0.00430 and 0.00175 respectively. As the temperature rises the values of the base normalized capacitance increases gradually. It can be seen that over the testing range the increase in base capacitance of C_z and C_j electrodes is about 6.56 times and 1.67 times respectively. The C_j base capacitance experienced less increase in the value because of the differential measurement of the capacitance in shear direction. However, as discussed, under hypothermal conditions about 1.5 °C change occurs in the temperature. For 1 °C change in temperature the approximate change in the base capacitance for C_z and C_j electrodes is about 3.53% and 13.59%. This error can be minimized using temperature calibration techniques.

8. Discussion

Although the article discusses the design, analysis and reliability and of the proposed sensor, there is still a room for discussion about the dielectric material choice which highly depends upon the application at hand. For laparoscopic RMIS procedures the acceptable sensing range is 0–5 N with a resolution of 0.01 N (Bandari *et al.*, 2020), 0–1.6 N with a resolution of 0.01 N (Gao *et al.*, 2023) are reported in the literature. The dielectric material properties such as Poisson's ratio, Young's modulus, density are the contributing factors which determine the force range of the sensor as the excitation electrode deflection depends upon how much the material is deformable under the required force range. The relative permittivity of the material contributes toward determining the sensitivity of the sensor.

These are the factors which were considered during the dielectric elastomer choice for the optimal force range. The sensor's cost of manufacturing is under $30 which makes it highly cost-effective and disposable after surgeries. The sensor's integration with the latest surgical robotic platforms (Korayem *et al.*, 2021; Korayem *et al.*, 2022; Korayem and Vahidifar, 2022; Najafinejad and Korayem, 2023) will further validate the sensor's usefulness and reliability.

9. Future work

The developed sensor has demonstrated promising results; however, further improvements can be achieved by optimizing the manufacturing process and addressing the misalignment of electrodes. This work primarily focuses on the conceptual discussion of the sensor. Future studies can include rigorous testing under varying humidity and temperature conditions, along with calibration of the sensor for such environments using advanced machine learning algorithms to enhance performance. Further efforts are under consideration to reduce the size of the sensor for seamless integration. Additional work may explore practical aspects such as manufacturing, commercialization and adoption in clinical applications.

10. Conclusion

In conclusion, this paper presents a novel flexible capacitive tactile force sensor designed for integration into surgical graspers for MIS and RMIS. The sensor's capacity to measure both normal and shear force contributes to heightened grasping stability and real-time feedback for surgeons undertaking intricate procedures. The sensor's unique design achieves inherent force decoupling and its compact size distinguishes it from existing designs in the literature. Fabricated through conventional machining and rapid prototyping techniques, the sensor exhibits cost-effectiveness and accessibility for widespread adoption. FEM simulations optimize the sensor's design, ensuring efficiency and reliability. Experimental validation demonstrates a decoupled and relatively linear response, with maximum force sensing ranges of 5 N in the normal force direction. Real-time response of the fabricated sensor along with stiffness assessment response represents the usability and effectiveness in detecting slippage and lumps during RMIS. The proposed sensor exhibits minimal hysteresis and excellent repeatability, showcasing its potential as an innovative tool to enhance precision and safety in minimally invasive surgical procedures.

References

Alleblas, C.C.J., Vleugels, M.P.H., Coppus, S.F.P.J. and Nieboer, T.E. (2017), "The effects of laparoscopic graspers with enhanced haptic feedback on applied forces: a randomized comparison with conventional graspers", *Surgical Endoscopy*, Vol. 31 No. 12, pp. 5411-5417, doi: 10.1007/s00464-017-5623-9.

Bandari, N., Dargahi, J. and Packirisamy, M. (2020), "Tactile sensors for minimally invasive surgery: a review of the state-of-the-art, applications, and perspectives", *IEEE Access*, Vol. 8, pp. 7682-7708, doi: 10.1109/ACCESS.2019.2962636.

Barrie, J., Russell, L., Hood, A.J., Jayne, D.G., Neville, A. and Culmer, P.R. (2018), "An in vivo analysis of safe laparoscopic grasping thresholds for colorectal surgery", *Surgical Endoscopy*, Vol. 32 No. 10, pp. 4244-4250, doi: 10.1007/s00464-018-6172-6.

Bechet, F., Ogawa, K., Sariyildiz, E. and Ohnishi, K. (2015), "Electrohydraulic transmission system for minimally invasive robotics", *IEEE Transactions on Industrial Electronics*, Vol. 62 No. 12, pp. 7643-7654, doi: 10.1109/TIE.2015.2453930.

Chatzipirpiridis, G., Erne, P., Ergeneman, O., Pané Vidal, S. and Nelson, B. (2015), "A magnetic force sensor on a catheter tip for minimally invasive surgery", doi: 10.1109/EMBC.2015.7320241

Dai, Y., Abiri, A., Liu, S., Paydar, O., Sohn, H., Dutson, E.P., Grundfest, W.S. and Candler, R. (2017), "Grasper integrated Tri-Axial force sensor system for robotic minimally invasive surgery", doi: 10.1109/EMBC.2017.8037717

Dargahi, J. (2000), "A piezoelectric tactile sensor with three sensing elements for robotic, endoscopic and prosthetic applications", *Sensors and Actuators*, Vol. 80 www.elsevier.nlrlocatersna

Feldheiser, A., Aziz, O., Baldini, G., Cox, B.P.B.W., Fearon, K.C.H., Feldman, L.S., Gan, T.J., Kennedy, R.H., Ljungqvist, O., Lobo, D.N., Miller, T., Radtke, F.F., Ruiz Garces, T., Schricker, T., Scott, M.J., Thacker, J.K., Ytrebø, L.M. and Carli, F. (2016), "Enhanced recovery after surgery (ERAS) for gastrointestinal surgery, part 2: consensus statement for anaesthesia practice", *Acta Anaesthesiologica Scandinavica*, Vol. 60 No. 3, doi: 10.1111/aas.12651.

Gao, H., Ai, X., Sun, Z., Chen, W. and Gao, A. (2023), "Progress in Force-Sensing techniques for surgical robots", *Journal of Shanghai Jiaotong University (Science)*, Vol. 28 No. 3, pp. 370-381, doi: 10.1007/s12204-023-2607-x.

Geneva, I.I., Cuzzo, B., Fazili, T. and Javaid, W. (2019), "Normal body temperature: a systematic review", *Open Forum Infectious Diseases*, Vol. 6 No. 4, doi: 10.1093/ofid/ofz032.

Hsieh, M.L., Yeh, S.K., Lee, J.H., Cheng, M.C. and Fang, W. (2021), "CMOS-MEMS capacitive tactile sensor with vertically integrated sensing electrode array for sensitivity enhancement", *Sensors and Actuators A: Physical*, Vol. 317, doi: 10.1016/j.sna.2020.112350.

Hussain, S., Saleem, M.M., Rehan, M., Elahi, H. and Tiwana, M.I. (2024), "A high sensitivity, low cost and fully decoupled multi-axis capacitive tactile force sensor for robotic surgical systems", *Plos One*, Vol. 19 No. 11, p. e0313737, doi: 10.1371/journal.pone.0313737.

Karmakar, R.S., Chu, C.P., Liao, Y.C. and Lu, Y.W. (2022), "PVA tactile sensors based on electrical contact resistance (ECR) change mechanism for subtle pressure detection", *Sensors and Actuators A: Physical*, Vol. 342, p. 113613, doi: 10.1016/J.SNA.2022.113613. (accessed 16 March 2024).

Kim, H.K., Lee, S. and Yun, K.S. (2011), "Capacitive tactile sensor array for touch screen application", *In Sensors and Actuators, A: Physical*, Vol. 165 No. 1, pp. 2-7, doi: 10.1016/j.sna.2009.12.031.

Kim, U., Kim, Y.B., Seok, D.Y., So, J. and Choi, H.R. (2018a), "A surgical palpation probe with 6-axis force/torque sensing capability for minimally invasive surgery", *IEEE Transactions on Industrial Electronics*, Vol. 65 No. 3, pp. 2755-2765, doi: 10.1109/TIE.2017.2739681.

Kim, U., Kim, Y.B., So, J., Seok, D.Y. and Choi, H.R. (2018b), "Sensorized surgical forceps for robotic-assisted minimally invasive surgery", *IEEE Transactions on Industrial Electronics*, Vol. 65 No. 12, pp. 9604-9613, doi: 10.1109/TIE.2018.2821626.

Kim, U., Lee, D.H., Yoon, W.J., Hannaford, B. and Choi, H. R. (2015), "Force sensor integrated surgical forceps for minimally invasive robotic surgery", *IEEE Transactions on Robotics*, Vol. 31 No. 5, pp. 1214-1224, doi: 10.1109/TRO.2015.2473515.

King, C.H., Culjat, M.O., Franco, M.L., Bisley, J.W., Carman, G.P., Dutson, E.P. and Grundfest, W.S. (2009), "Short contributions: a multielement tactile feedback system for robot-assisted minimally invasive surgery", *IEEE Transactions on Haptics*, Vol. 2 No. 1, pp. 52-56, doi: 10.1109/TOH.2008.19.

Korayem, M.H. and Vahidifar, V. (2022), "Detecting hand's tremor using leap motion controller in guiding surgical robot arms and laparoscopic scissors", *Measurement*, Vol. 204, p. 112133, doi: 10.1016/J.MEASUREMENT.2022.112133. (accessed 24 November 2024).

Korayem, M.H., Madihi, M.A. and Vahidifar, V. (2021), "Controlling surgical robot arm using leap motion controller with Kalman filter", *Measurement*, Vol. 178, p. 109372, doi: 10.1016/J.MEASUREMENT.2021.109372. (accessed 24 November 2024).

Korayem, M.H., Vosoughi, R. and Vahidifar, V. (2022), "Design, manufacture, and control of a laparoscopic robot via leap motion sensors", *Measurement*, Vol. 205, p. 112186, doi: 10.1016/J.MEASUREMENT.2022.112186 (accessed 24 November 2024).

Krishna, G.M. and Rajanna, K. (2025), "23.3: tactile sensor based on piezoelectric resonance".

Lanfranco, A.R., Castellanos, A.E., Desai, J.P. and Meyers, W. C. (2004), "Robotic surgery: a current perspective", *Annals of Surgery*, Vol. 239 No. 1, doi: 10.1097/01.sla.0000103020.19595.7d.

Lee, D.H., Kim, U., Moon, H., Koo, J.C., Yoon, W.J. and Choi, H.R. (2025), "Preliminary design of Multi-Axial contact force sensor for minimally invasive robotic surgery grasper".

Lee, D.H., Kim, U., Gulrez, T., Yoon, W.J., Hannaford, B. and Choi, H.R. (2016), "A laparoscopic grasping tool with force sensing capability", *IEEE/ASME Transactions on Mechatronics*, Vol. 21 No. 1, pp. 130-141, doi: 10.1109/TMECH.2015.2442591.

Li, T., Shi, C. and Ren, H. (2018), "A High-Sensitivity tactile sensor array based on fiber Bragg grating sensing for tissue palpation in minimally invasive surgery", *IEEE/ASME Transactions on Mechatronics*, Vol. 23 No. 5, pp. 2306-2315, doi: 10.1109/TMECH.2018.2856897.

Naidu, A.S., Patel, R.V. and Naish, M.D. (2017), "Low-Cost disposable tactile sensors for palpation in minimally invasive surgery", *IEEE/ASME Transactions on Mechatronics*, Vol. 22 No. 1, pp. 127-137, doi: 10.1109/TMECH.2016.2623743.

Najafinejad, A. and Korayem, M.H. (2023), "Detection and minimizing the error caused by hand tremors using a leap motion sensor in operating a surgeon robot", *Measurement*, Vol. 221, p. 113544, doi: 10.1016/J.MEASUREMENT.2023.113544 (accessed 24 November 2024).

Najarian, S., Dargahi, J. and Zheng, X.Z. (2006), "A novel method in measuring the stiffness of sensed objects with applications for biomedical robotic systems", *The International Journal of Medical Robotics and Computer Assisted Surgery*, Vol. 2 No. 1, pp. 84-90, doi: 10.1002/rcs.75.

Othman, W., Lai, Z.H.A., Abril, C., Barajas-Gamboa, J.S., Corcelles, R., Kroh, M. and Qasaimeh, M.A. (2022a), "Tactile sensing for minimally invasive surgery: conventional methods and potential emerging tactile technologies", *Frontiers in Robotics and AI*, Vol. 8, p. 705662, doi: 10.3389/frobt.2021.705662.

Othman, W., Vandyck, K.E., Abril, C., Barajas-Gamboa, J.S., Pantoja, J.P., Kroh, M. and Qasaimeh, M.A. (2022b), "Stiffness assessment and lump detection in minimally invasive surgery using In-House developed smart laparoscopic forceps", *IEEE Journal of Translational Engineering in Health and Medicine*, Vol. 10, doi: 10.1109/JTEHM.2022.3180937.

Rehan, M., Saleem, M.M., Tiwana, M.I., Shakoor, R.I. and Cheung, R. (2022), "A soft multi-axis high force range magnetic tactile sensor for force feedback in robotic surgical systems", *Sensors*, Vol. 22 No. 9, doi: 10.3390/s22093500.

Rivero-Moreno, Y., Echevarria, S., Vidal-Valderrama, C., Stefano-Pianetti, L., Cordova-Guilarte, J., Navarro-Gonzalez, J., Acevedo-Rodríguez, J., Dorado-Avila, G., Osorio-Romero, L., Chavez-Campos, C. and Acero-Alvarracín, K. (2023), "Robotic surgery: a comprehensive review of the literature and current trends", *Cureus*, Vol. 15 No. 7, doi: 10.7759/cureus.42370.

Roriz, P., Frazão, O., Lobo-Ribeiro, A.B., Santos, J.L. and Simões, J.A. (2013), "Review of fiber-optic pressure sensors for biomedical and biomechanical applications", *Journal of Biomedical Optics*, Vol. 18 No. 5, p. 050903, doi: 10.1117/1.jbo.18.5.050903.

Sastry, S.S., Cohn, M. and Tendick, F. (1997), "Milli-robotics for remote, minimally invasive surgery", *Robotics and Autonomous Systems*, Vol. 21 No. 3, pp. 305-316. , available at: http://robotics.eecs.berkeley.edu/~lara/medical.html

Sedaghati, R., Dargahi, J. and Singh, H. (2005), "Design and modeling of an endoscopic piezoelectric tactile sensor", *International Journal of Solids and Structures*, Vol. 42 Nos 21/22, pp. 5872-5886, doi: 10.1016/j.ijsolstr.2005.03.029.

Simaan, N., Yasin, R.M. and Wang, L. (2018), "Medical technologies and challenges of Robot-Assisted minimally invasive intervention and diagnostics", *Annual Review of Control, Robotics, and Autonomous Systems*, Vol. 1 No. 1, pp. 465-490, doi: 10.1146/annurev-control-060117-104956.

Sokhanvar, S., Packirisamy, M. and Dargahi, J. (2007), "A multifunctional PVDF-based tactile sensor for minimally invasive surgery", *Smart Materials and Structures*, Vol. 16 No. 4, pp. 989-998, doi: 10.1088/0964-1726/16/4/006.

Takahashi, H., Nakai, A., Thanh-Vinh, N., Matsumoto, K. and Shimoyama, I. (2013), "A triaxial tactile sensor without crosstalk using pairs of piezoresistive beams with sidewall

doping", *Sensors and Actuators A: Physical*, Vol. 199, pp. 43-48, doi: 10.1016/j.sna.2013.05.002.

Tanaka, M., Furubayashi, M., Tanahashi, Y. and Chonan, S. (2000), "Development of an active palpation sensor for detecting prostatic cancer and hypertrophy".

Tiwana, M.I., Redmond, S.J. and Lovell, N.H. (2012), "A review of tactile sensing technologies with applications in biomedical engineering", *Sensors and Actuators A: Physical*, Vol. 179, pp. 17-31, doi: 10.1016/j.sna.2012.02.051.

Vaicekauskaite, J., Mazurek, P., Vudayagiri, S. and Skov, A.L. (2020), "Mapping the mechanical and electrical properties of commercial silicone elastomer formulations for stretchable transducers", *Journal of Materials Chemistry C*, Vol. 8 No. 4, pp. 1273-1279, doi: 10.1039/c9tc05072h.

Wanninayake, I.B. (2019), "Miniaturised optical fibre based palpations instrument for minimally invasive surgery", *Journal of Physics: Conference Series*, Institute of Physics Publishing, Vol. 1151, doi: 10.1088/1742-6596/1151/1/012014.

Yu, L., Yan, Y., Yu, X. and Xia, Y. (2018), "Design and realization of forceps with 3-D force sensing capability for Robot-Assisted surgical system", *IEEE Sensors Journal*, Vol. 18 No. 21, pp. 8924-8932, doi: 10.1109/JSEN.2018.2867838.

Zhu, Y., Chen, X., Chu, K., Wang, X., Hu, Z. and Su, H. (2022), "Carbon black/PDMS based flexible capacitive tactile sensor for Multi-Directional force sensing", *Sensors*, Vol. 22 No. 2, p. 628, doi: 10.3390/s22020628.

Corresponding author

Muhammad Mubasher Saleem can be contacted at: mubasher.saleem@mu.ie